Applied Physics B (2018) 124:91
https://doi.org/10.1007/s00340-018-6959-0

Applied Physics B
Lasers and Optics

Optical frequency comb generation based on the dual-mode square microlaser and a nonlinear fiber loop

Hai-Zhong Weng[1] · Jun-Yuan Han[1] · Qing Li[2] · Yue-De Yang[1] · Jin-Long Xiao[1] · Guan-Shi Qin[2] · Yong-Zhen Huang[1]

Received: 24 January 2018 / Accepted: 21 April 2018 / Published online: 3 May 2018

Abstract
A novel approach using a dual-mode square microlaser as the pump source is demonstrated to produce wideband optical frequency comb (OFC). The enhanced nonlinear frequency conversion processes are accomplished in a nonlinear fiber loop, which can reduce the stimulated Brillouin scattering threshold and then generate a dual-mode Brillouin laser with improved optical signal-to-noise ratio. An OFC with 130 nm bandwidth and 76 GHz repetition rate is successfully generated under the four-wave mixing, and the number of the comb lines is enhanced by ~ 26 times compared with the system without fiber loop. In addition, the repetition rate of the comb can be adjusted by changing the injection current of the microlaser. The pulse width of the comb spectrum is also compressed from 3 to 1 ps with an extra amplification-nonlinear process.

1 Introduction

Optical frequency combs (OFCs) have attracted a great deal of interest for their applications in optical clocks [1], molecular fingerprinting [2], microwave photonic [3], optical arbitrary waveform generation [4], and dense wavelength division multiplexing [5], etc. Compared with the traditional femtosecond mode-locked lasers [6], OFCs with high repetition rate can be generated by injecting a continuous-wave (CW) light into a high-quality-factor microresonator with large free spectra range [7]. Different repetition rates from 16 to 850 GHz were realized by changing the cavity size [7–9], which can be applied in astronomic spectra calibration and THz wave generation. In addition, the OFCs generated by two separate pump laser sources and highly nonlinear fibers (HNLFs), which have high and tunable repetition rates, were also demonstrated for narrow pulse generation and optical communication [10–12]. For realizing a chip-integrated comb, an on-chip dual-wavelength laser source with narrow linewidth and high power is required. Dual-wavelength semiconductor lasers with a frequency difference at THz have been demonstrated, such as integrated dual-mode DFB or DBR lasers [13, 14].

Recently, we realized a stable dual-mode lasing in a single square microcavity laser and demonstrated a strong mode correlation between the two lasing modes [15]. Dual-mode square microlaser replacing the separated pump sources to generate OFC was also verified in [16], while the degradation of the comb tooth linewidth reduced the parameter conversion efficiency. Moreover, the stimulated Brillouin scattering (SBS) effect wasted the pump energy and resulted in a limitation of comb generation. It will inevitably introduce the amplified spontaneous emission noise (ASE) and reduce the optical signal-to-noise ratio (OSNR) when further increasing the pump power. Brillouin effect was successfully exploited to generate ultra-narrow linewidth single-longitudinal-mode Brillouin fiber laser due to the narrowing effect of the Stokes lasing [17]. The Brillouin laser sources with improved performance were also exploited to generate broadband OFC with the electro-optic modulation or the fiber four-wave-mixing (FWM) techniques [18, 19].

In this work, a nonlinear fiber loop configuration using dual-mode square microlaser as pump source is proposed and experimentally demonstrated for generating wideband

This article is part of the topical collection "Mid-infrared and THz Laser Sources and Applications" guest edited by Wei Ren, Paolo De Natale and Gerard Wysocki.

✉ Yong-Zhen Huang
yzhuang@semi.ac.cn

[1] State Key Laboratory of Integrated Optoelectronics, Institute of Semiconductors, College of Materials Science and Opto-Electronic Technology, University of Chinese Academy of Sciences, Chinese Academy of Sciences, Beijing 100083, China

[2] State Key Laboratory of Integrated Optoelectronics, College of Electronic Science and Engineering, Jilin University, 2699 Qianjin Street, Changchun 130012, China

OFCs. Owing to the long fiber loop and the high nonlinear coefficient, the SBS threshold is reduced and a dual-mode Brillouin fiber laser with improved OSNR is generated, leading to an increased number of the comb lines in the OFC generation.

2 Lasing performance of dual-mode square microlaser

Dual-mode square microlaser with a side length of 24 μm and a 1.5 μm-wide waveguide connected to the square vertex is adopted, using the same geometry as in [15]. The laser is fabricated using an AlGaInAs/InP wafer with six pairs of compressively strained AlGaInAs multiple-quantum wells, with the fabrication process similar to that in [20]. Then the lasing characteristics are measured by butt-coupling a tapered single-mode fiber to the cleaved waveguide facet. The output power and applied voltage versus the CW injection current are measured at the temperature of 288 K and plotted in Fig. 1a. The threshold current is about 8 mA and the maximum coupled power is 0.39 mW at 56 mA. A resistance of 13.7 Ω is estimated for the device by fitting the voltage–current curve.

The lasing spectra at different injection currents are measured by an optical spectrum analyzer (OSA) with a resolution of 0.02 nm and represented in Fig. 1b. The spectrum at 50 mA shows three main longitudinal modes around 1540, 1550 and 1560 nm. A longitudinal mode interval of ~9.7 nm can be analytically obtained by $\lambda^2/2\sqrt{2}an_g$ with the group index $n_g$of 3.65 around 1550 nm, which agree well with the experimental results [21]. Several lines are depicted to track the main lasing wavelength variation with the current, where the circle, triangle and square symbols correspond to the fundamental (0th-order), first-order (1st-order) and second-order (2nd-order) transverse modes, respectively. The redshifts of lasing wavelengths are attributed to an injection current induced thermal effect, which also results in the redshift of gain spectrum and thus the mode hopping. The 0th-order transverse mode first lases at 1538.9 nm as the current is 10 mA, and then jumps to the next longitudinal mode at the long wavelength side when the current increases to 20 mA due to the redshift of gain spectrum. For the 1st-order mode, mode hopping can be observed at 40 and 60 mA, respectively. As the current increases from 50 to 60 mA, the 2nd-order transverse mode jumps 19.8 nm over two longitudinal mode intervals, due to the lower mode Q factor around 1550 nm. Dual-transverse-mode lasing with the mode intervals of 0.82, 0.61 and 0.95 nm can be achieved around 1539, 1550 and 1560 nm, when the currents are 40, 50 and 70 mA, respectively. Therefore, dual-mode lasing with variable mode spacing can be realized in one laser by adjusting the injection current with an optical filter to filter out the undesired peaks.

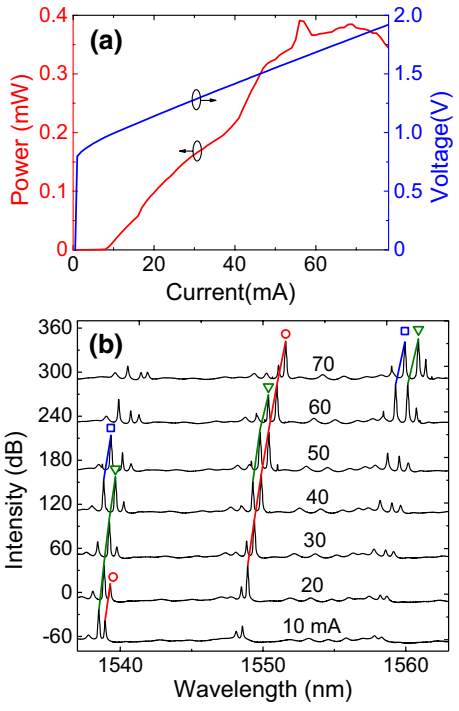

Fig. 1 **a** Measured *L–I–V* curve for a 24-μm-side-length square microlaser with a 1.5-μm-wide output waveguide. **b** Lasing spectra at different currents with the marked lines indicating the same mode

3 Generation of wideband optical frequency comb

3.1 Experimental setup

The experimental setup of the proposed OFC generator is shown in Fig. 2a. The laser emission is first pre-amplified by an erbium-doped fiber amplifier (EDFA) and filtered with an optical band pass filter (OBPF) to select the two desired lasing modes and reduce the ASE noise. Then the filtered output light is amplified by a high-power EDFA and injected into a 500-m-long highly nonlinear fiber through optical circulator 1 (OC1), and the transmitted wave is detected at monitoring point a, i.e, the port 3 of OC2. When the pump power exceeds the SBS threshold, the backward Brillouin Stokes (BS) wave with a frequency shift ω_{SBS} of 9.33 GHz is generated and collected at monitoring point b, i.e, port 3 of the OC1. The OSAs and power meters (PMs) are set in the monitors to detect corresponding signals. This is the system without nonlinear fiber loop (NLFL), which is similar as the first-stage of the configuration shown in [16]. Then the NLFL is constructed by injecting the BS signals back into the HNLF via OC2, as the red dashed transmitted line

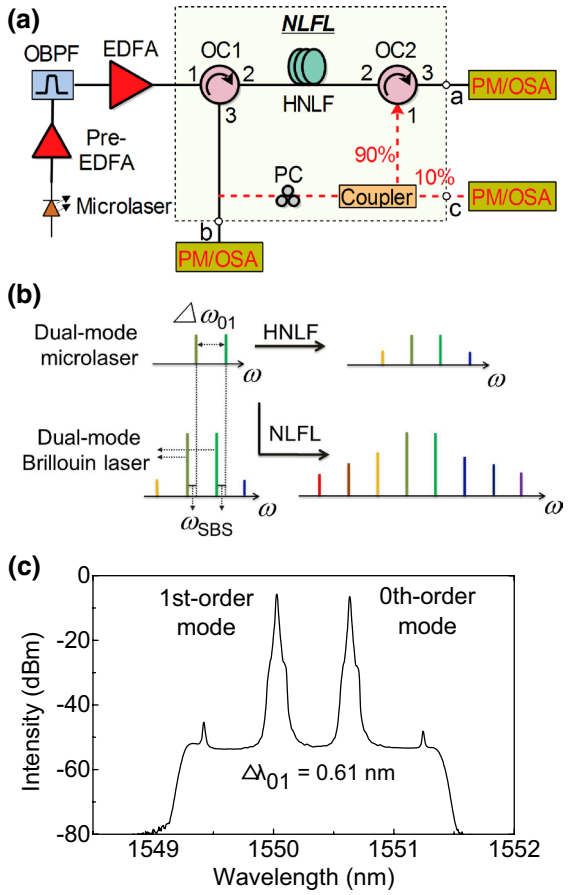

Fig. 2 **a** The NLFL experimental setup for generating OFC. *EDFA* erbium-doped fiber amplifier, *OBPF* optical band pass filter, *HNLF* highly nonlinear fiber, *OC* optical circulator, *PC* polarization controller, *OSA* optical spectrum analyzer, *PM* power meter. **b** The schematic comparison between the methods with and without fiber loop. **c** Filtered output of the microlaser at the current of 53 mA

shows. A polarization controller (PC) is utilized to adjust the polarization states of the Stokes waves to achieve the maximum Brillouin gain in the loop. 90% of the BS power is injected into the port 1 of OC2, and the remaining 10% is extracted for monitoring. Therefore, the generated BS waves will circulate along the loop in the counter-clockwise (CCW) direction and interact with the pump waves, which will increase the pump power conversion efficiency and reduce the SBS threshold. The HNLF used in the experiments has a nonlinear coefficient of ~ 10 W^{-1} km^{-1}, a zero dispersion wavelength of ~ 1535 nm, and a dispersion slope of ~ 0.022 ps nm^{-2} km^{-1}.

Figure 2b schematically shows the comparison between the methods with and without NLFL. When the fiber loop is disconnected, the dual-mode square microlaser can act as the pump source and initiate the FWM in the HNLF. This can be seen as a travelling-wave FWM process with low wavelength conversion efficiency due to the SBS effect. However, the NLFL approach can generate a dual-mode Brillouin laser with improved OSNR, which can act as the new pump source for the synchronous mixing process and lead to a broadband optical comb. It should be noticed that mode interval of the generated Brillouin laser is equal to the repetition rate of the comb, which are determined by the mode interval of the dual-mode square microlaser. The employment of the NLFL can not only generate a dual-mode Brillouin laser with improved performance, but also enhance the wavelength conversion efficiency.

Figure 2c shows the filtered output spectrum of the dual-mode microlaser at the injection current of 53 mA, which act as the pump source. The two lasing peaks at 1550.62 and 1550.01 nm correspond to the 0th-order and the 1st-order transverse mode, respectively. The mode interval is 0.61 nm, and the OSNR is as high as 47 dB almost equaling to that of the microlaser. A pair of FWM peaks is clearly seen at 1551.23 and 1549.4 nm, which indicates the coexistence of the dual-mode lasing.

3.2 Results and discussion

We first consider the system without NLFL and represent the experimental results in Fig. 3, using the laser output of Fig. 2c. In Fig. 3a, the measured transmitted power and backward BS power versus the pump power are depicted with square and circle symbols, respectively. The SBS threshold is about 20 dBm and the reflected power exceeds the transmitted power as the pump power exceeds 27 dBm. Fitting the BS power with linear function in linear coordinate, we obtain a Brillouin gain efficiency of 36%. The Brillouin scattering will consume the pump power and severely limit the wavelength conversion efficiency in the forward direction. Figure 3b shows the measured transmitted spectra at monitor a under different pump powers, which have several comb teeth with equal frequency interval due to the FWM effect. The teeth number gradually increases from 6 to 9 as the pump power increases from 20 to 27 dBm. As discussed in [16], further increasing the pump power could not broaden the comb range anymore due to the SBS effect accompanied with large ASE noise. For the backward Stokes waves, the spectra versus the pump powers are summarized in Fig. 3c, with two dashed lines marked for the two original pump wavelengths. Two BS lasing peaks are generated when the pump power increases to 20 dBm, and the wavelength offset from the dashed lines are 0.075 nm, which corresponds to a Brillouin frequency shift of 9.33 GHz. Most power transfer into the BS waves and the dual-mode Brillouin laser is generated when further increasing the pump power. The FWM sidebands of the Brillouin laser are also observed. Comparing the spectra of the two directions, one can find that the OSNRs of the Brillouin lasers are about 10 dB larger than

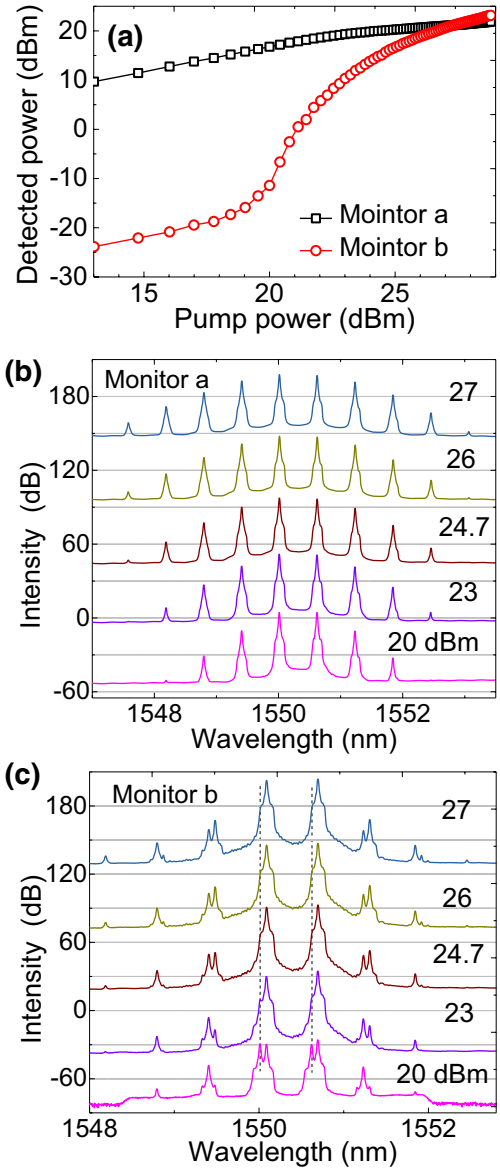

Fig. 3 **a** Detected powers at monitors a and b versus the pump powers for the system without NLFL. **b, c** Measured spectra at different pump powers for the transmitted signal and the backward Stokes waves, respectively

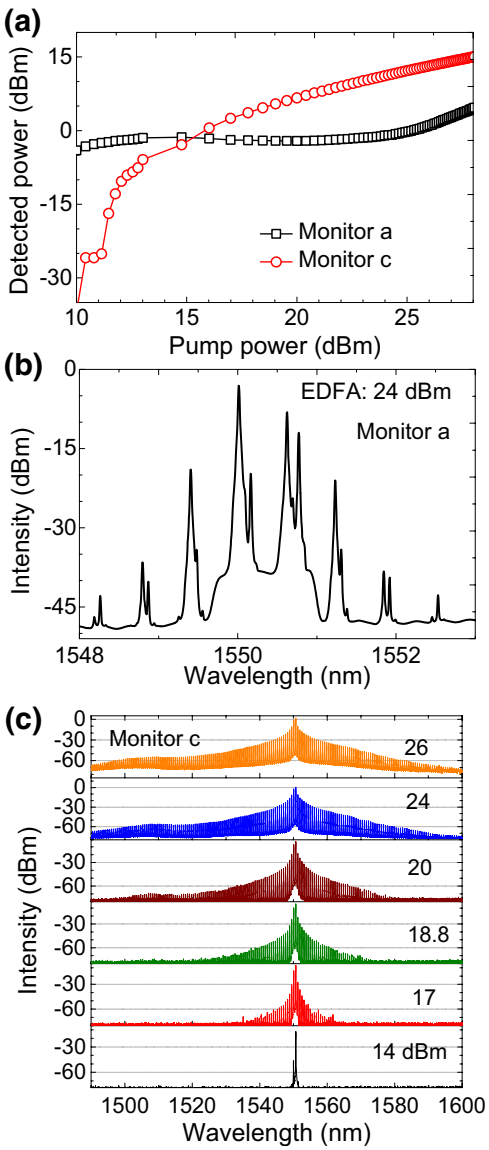

Fig. 4 **a** Detected powers at monitors a and c versus the pump powers for the approach with NLFL. **b** Measured transmitted spectrum as the pump power is 24 dBm. **c** Measured CCW spectra under different pump powers

those of the original lasing mode and the forward transmission signal.

When the fiber loop is closed, we detect the powers of the transmitted and CCW signals and plot them in Fig. 4a. For the NLFL system, the power in the CCW direction is larger than the transmitted power as the pump power is larger than 15 dBm, which is 12 dB lower than the value in Fig. 3a. Figure 4b gives the measured transmitted spectrum at the pump power of 24 dBm, which is composed by the original pump waves and the 2nd-order Stokes waves from the loop. The spectrum linewidth of the Stokes waves are clearly narrower than the linewidths of the mixing sidebands. As the CCW spectra shown in Fig. 4c, a lasing peak at 1550.69 nm with OSNR of 60 dB is obtained at 14 dBm pump power, which is the 1st-order Stokes wave of the 0th-order mode. With gradually increasing the pump power, the intensity of the 1st-order mode also reaches the SBS threshold and generates a BS wave. Therefore, dual-mode Brillouin lasers with improved OSNRs could be generated with a lower threshold than Fig. 3b, with the mode interval same as that of the dual-mode microlaser. As the power increases further, multi-wavelength spectra with a constant frequency separation of 76.25 GHz is generated by the nonlinear interaction between the two BS waves via cascaded FWM. At the pump

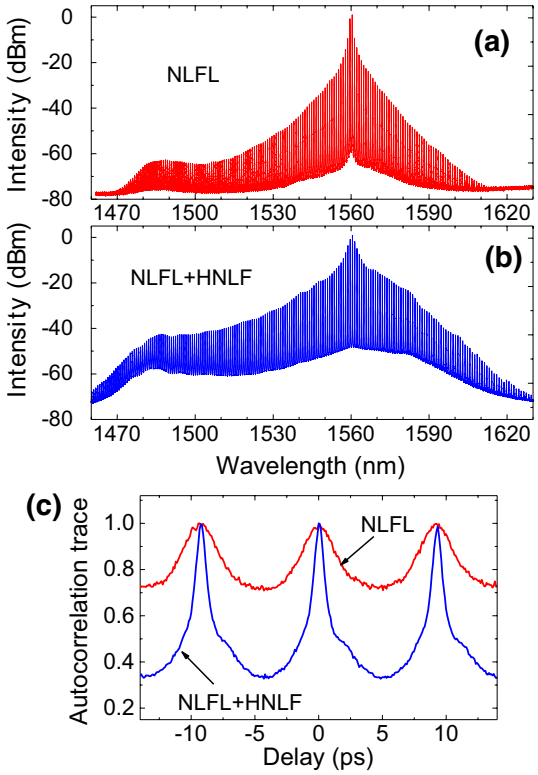

Fig. 5 **a** Measured OFC spectra with NLFL, **b** with NLFL and an additional amplification-nonlinear as the square laser is injected with 63 mA. **c** Autocorrelation traces

power of 24 dBm, OFC with 130 nm bandwidth is produced, which is about 26 times the teeth number given in Fig. 3b. The frequency separation of the dual-mode Brillouin lasers and the ω_{SBS} are multiple of the cavity-free spectral range (FSR $\approx$ 400 kHz). We also calculated the Q factor and the finesse of the cavity without Brillouin gain [18], and the corresponding values are about 2.1×10^9 and 3.8, respectively. These results indicate that the dual-mode Brillouin laser can be generated due to the enhanced Brillouin effect in the NLFL, which can also increase the FWM efficiency greatly.

3.3 Varied repetition rates and time domain results

As discussed in Fig. 1b, the lasing wavelengths and mode intervals can be tuned by adjusting the currents. When the laser is injected with a current of 63 mA, the lasing modes are the 1st-order and 2nd-order transverse modes and the wavelengths are 1560.35 and 1559.48 nm, respectively. Using this dual-mode lasing source as the comb seed and the NLFL system, we obtain another OFC and plot the spectrum (Fig. 5a), with the pump power of 24 dBm. The repetition rate is 107 GHz, which is larger than that shown in Fig. 4. However, the intensity of the pump sources are about 10 dB larger than the other teeth and the spectrum flatness is need to be improved. By amplifying the spectrum with another EDFA and injecting into another 500-m-long HNLF, an OFC spectrum exceeding 150 nm is realized and plotted in Fig. 5b. The bandwidth is not broadened obviously after the second spread spectrum stage because that the intensity of the comb teeth decrease rapidly. A great part of the sidebands cannot be amplified due to the large ASE noise in the second high-power EDFA.

Figure 5c shows the measured autocorrelation traces of the generated OFCs, where the average pulse period maintains at 9.3 ps. The signal from the NLFL appears nearly unmodulated in time domain due to the large intensity difference between the pump waves and the sidebands. A clear pulse-like trace is observed after the second amplification-nonlinear stage because the intensity differences are reduced and the spectrum bandwidth is broadened. According to the Gaussian fitting, the pulse width is compressed from 3 to 1 ps. Even though various repetition rates can be realized using the different longitudinal modes, dual-mode lasing source with a continuously tunable and controllable mode interval is still anticipated. Deformed cavities and differentiated injection for the two transverse lasing modes are considered to fulfill this purpose.

4 Conclusions

In summary, we have proposed and demonstrated the wideband OFC generation based on the nonlinear fiber loop. The dual-mode square microlaser with variable mode spacing is used as the comb seed. With the fiber loop, dual-mode Brillouin laser with improved performance is generated and the FWM efficiency is enhanced. The bandwidth of the comb spectrum is increased about 26 times. By adjusting the injection current of the dual-mode laser, the OFCs with sub-THz repetition rates are demonstrated. The pulse width of the OFC is also compressed from 3 to 1 ps with an additional amplification-nonlinear process. These results have shown potential of the present dual-mode square microlaser for realizing the wideband optical comb.

Acknowledgements This work was supported by the National Natural Science Foundation of China under Grant nos. 61527823, and 61377105.

References

1. T. Udem, R. Holzwarth, T.W. Hansch, Nature **416**, 233–237 (2002)
2. M.J. Thorpe, K.D. Moll, R.J. Jones, B. Safdi, J. Ye, Science **311**, 1595–1599 (2006)
3. V. Torres-Company, A.M. Weiner, Laser Photon. Rev. **8**, 368–393 (2014)

4. Z. Jiang, D.E. Leaird, A.M. Weiner, J. Lightwave Technol. **24**, 2487–2494 (2006)
5. P.J. Delfyett, S. Gee, M.T. Choi, H. Izadpanah, W. Lee, S. Ozharar, F. Quinlan, T. Yilmaz, J. Lightwave Technol. **24**, 2701–2719 (2006)
6. D.J. Jones, S.A. Diddams, J.K. Ranka, A. Stentz, R.S. Windeler, J.L. Hall, S.T. Cundiff, Science **288**, 635–639 (2000)
7. T.J. Kippenberg, R. Holzwarth, S. Diddams, Science **332**, 555–559 (2011)
8. P. Del'Haye, T. Herr, E. Gavartin, M. Gorodetsky, R. Holzwarth, T.J. Kippenberg, Phys. Rev. Lett. **107**, 063901 (2011)
9. P. Del'Haye, A. Coillet, T. Fortier, K. Beha, D.C. Cole, K.Y. Yang, H. Lee, K.J. Vahala, S.B. Papp, S.A. Diddams, Nat. Photon. **10**, 516–520 (2016)
10. J. Fatome, S. Pitois, G. Millot, IEEE J. Quantum Electron. **42**, 1038–1046 (2006)
11. V. Ataie, E. Myslivets, B.P.P. Kuo, N. Alic, S. Radic, J. Lightwave Technol. **32**, 840–846 (2014)
12. E. Myslivets, B.P.P. Kuo, N. Alic, S. Radic, Opt. Express **20**, 3331–3344 (2012)
13. A. Klehr, J. Fricke, A. Knauer, G. Erbert, M. Walther, R. Wilk, M. Mikulics, M. Koch, IEEE J. Sel. Top. Quantum Electron. **14**, 289–294 (2008)
14. S. Hoffmann, M. Hofmann, M. Kira, S.W. Koch, Semicond. Sci. Technol. **20**, S205–S210 (2005)
15. H.Z. Weng, Y.Z. Huang, X.W. Ma, F.L. Wang, M.L. Liao, Y.D. Yang, J.L. Xiao, IEEE Photon.Technol. Lett. **29**, 1931–1934 (2017)
16. H.Z. Weng, Y.Z. Huang, X.W. Ma, Y.D. Yang, J.L. Xiao, J.Y. Han, M.L. Liao, IEEE Photon. J. **10**, 7102009 (2018)
17. J.F. Zhao, C. Zhang, Z.H. Li, C.Y. Miao, H. Gu, Z.R. Tong, X.D. Sun, J.J. Bai, Laser Phys. **24**, 105102 (2014)
18. Q. Li, Z.X. Jia, Z.R. Li, Y.D. Yang, J.L. Xiao, S.W. Chen, G.S. Qin, Y.Z. Huang, W.P. Qin, AIP Adv. **7**, 075215 (2017)
19. K.M. Imrul, M. Rochette, Opt. Lett. **42**, 2718–2721 (2017)
20. Y.D. Yang, Y.Z. Huang, J. Phys. D Appl. Phys. **49**, 253001 (2016)
21. L.X. Zou, Y.Z. Huang, X.M. Lv, H. Long, J.L. Xiao, Y. Du, Appl. Phys. B **117**, 453–458 (2014)